This is an Accepted Manuscript of an article published by Royal Society of Chemistry in CrystEngComm on 18 Jan 2023, available online: 10.1039/d2ce01470j

4,4’-Biphenyldisulfonic acid induced coordination polymers of symmetrical tetramethyl cucurbit[6]uril with alkaline-earth metals for detection of antibiotics

Kai Chen[a]*, Zhao-Qiang Zhu[a], Ming-Hui Zhang[a], Chen Chen[a], Jing-Xin Liu[b]*, Jing-Xin Liu[b]*
Carl Redshaw[d]

[a] *Collaborative Innovation Center of Atmospheric Environment and Equipment Technology; Jiangsu Key Laboratory of Atmospheric Environment Monitoring and Pollution Control; Nanjing University of Information Science & Technology, Nanjing 210044, P. R. China. Email: catqchen@163.com*

[b] *College of Chemistry and Chemical Engineering, Anhui University of Technology, Maanshan 243002, China. Email: jxliu411@163.com*

[c] Plastics Collaboratory, Department of Chemistry, University of Hull, Hull HU6 7RX, UK.

Abstract: Three coordination polymers based on the macrocyclic symmetrical tetramethyl cucurbit[6]uril (TMeQ[6]) with formulae $\{[Ca(C_{30}H_{30}N_{20}O_{10})_2Cl_2]Cl_2(H_2O)_2\}\cdot 12H_2O$ (**1**), $\{[Sr(C_{30}H_{30}N_{20}O_{10})_2Cl_2]Cl_2(H_2O)_2\}\cdot 12H_2O$ (**2**) and $\{[Ba(C_{30}H_{30}N_{20}O_{10})_2Cl_2]Cl_2(H_2O)_2\}\cdot 12H_2O$ (**3**) have been obtained by the self-assembly of TMeQ[6] with the corresponding alkaline-earth metal salts in the presence of 4,4’-biphenyldisulfonic acid (BPDS). Single crystal X-ray diffraction analysis of these three coordination polymers reveals that the deprotonated 4,4’-biphenyldisulfonic acid ($BPDS^{2-}$) plays an important role in the self-assembly of these coordination polymers. In complexes **1** and **2**, only the TMeQ[6] is involved in coordination with the Ca^{2+} and Sr^{2+} ions. The $BPDS^{2-}$ is incorporated into the “outer-surface interactions” with the TMeQ[6]. While in complex **3**, the $BPDS^{2-}$ is also coordinated with the Ba^{2+} ion. These coordination polymers provide a new strategy to design and construct Q[*n*]-based poly-dimensional coordination polymers. Furthermore, complex **1** can selectively detect NFX (norfloxacin) molecules.

***Keywords*:** Alkaline-earth metals; 4,4’-Biphenyldisulfonic acid; Coordination polymer; Symmetrical tetramethyl cucurbit[6]uril; X-ray Crystallography.

Introduction

Antibiotic misuse can cause serious health problems and environmental pollution, and such issues have alarmed the scientific community[1,2]. With this in mind, efficiently and selectively identifying antibiotics is a key issue[3]. Various methods and materials have been employed to detect antibiotics, such as electrochemical methods, infrared spectroscopy, and liquid chromatography[4-6]. However, such methods suffer from high-cost, complex operation, are time-consuming, possess low sensitivity, and poor-portability problems, all of which restricts them for further development. Herein, we show that luminescence-based chemical sensor-based methods have great advantages such as high efficiency, low cost, simple operation, fast response, etc[7-13].

Metal-organic frameworks (MOFs) continue to attract attention as one type of chemical sensor. Among these materials, they often consist of multi-aromatic compounds. For their luminescence properties, they have often been voted the most promising candidate species[14-16]. Metallo-macrocyclic-based coordination polymers fabricated by self-assembled macrocyclic ligands with metal cations have also attracted much interest from many manufacturers because of their potential applications in sensors. As a family of macrocyclic ligands with an intramolecular cavity and two carbonyl-laced portals, cucurbit[*n*]urils (Q[*n*]s, *n* = 5–8, 10, 14)[17-23] are widely used to coordinate with various metal ions. From a structural viewpoint, the coordination of Q[*n*] with metal ions tends to generate low-dimensional structures, such as discrete molecular capsules and 1D chains. Recently, our group and others found that the addition of some small organic aromatic molecules (the third species) very often leads to the formation of Q[*n*]-based poly-dimensional coordination polymers. However, the final structure using such a method tends to be unpredictable and uncontrollable because these small organic aromatic molecules only act as inducers, and are not involved in metal coordination. Therefore, it is still a challenge to design and construct Q[*n*]-based poly-dimensional coordination polymers.

In the course of our ongoing studies on Q[*n*]-based coordination polymers, we have been interested in Q[*n*] derivatives and new types of organic aromatic molecules containing differing functionality. Symmetrical tetramethyl-cucurbit[6]uril (TMeQ[6]), a derivative of Q[6], possesses an ellipsoidal hydrophobic cavity and exhibits moderate solubility in aqueous media.[21] 4,4'-Biphenyldisulfonic acid (BPDS) is an organic aromatic molecule with two sulfonic groups located at its ends. We envisaged that the BPDS could be incorporated into the construction of TMeQ[6] with metal ions, and eventually form poly-dimensional coordination polymers. In the present study, we report the single-crystal X-ray structures of three coordination polymers, namely $\{[Ba(C_{30}H_{30}N_{20}O_{10})_2Cl_2]Cl_2(H_2O)_2\}\cdot 12H_2O$ (**1**),

{[Ca($C_{30}H_{30}N_{20}O_{10}$)$_2$$Cl_2$]$Cl_2$($H_2O$)$_2$}·12$H_2O$ (**2**), and {[Ba($C_{30}H_{30}N_{20}O_{10}$)$_2$$Cl_2$]$Cl_2$($H_2O$)$_2$} (**3**), which are self-assembled by the symmetrical tetramethyl-cucurbit[6]uril (TMeQ[6]) with the corresponding alkali-earth metal salts in the presence of BPDS (Scheme 1). These coordination polymers represent good examples of tuning Q[*n*]-based crystal structures by a third species.

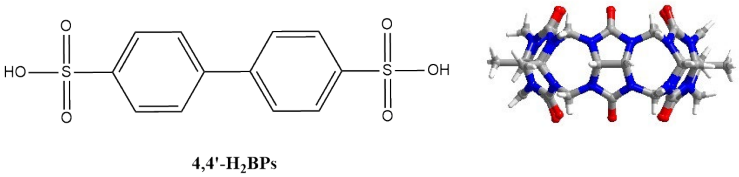

4,4'-H_2BPs

Scheme 1. Molecular structure of 4,4'-biphenyldisulfonic acid (H_2BPDS) and TMeQ[6].

Experimental Section

Materials and Methods

All the reagents and solvents employed were commercially available and used as received without further purification. TMeQ[6] was synthesized by published procedures[24].

Syntheses

{[Ca($C_{30}H_{30}N_{20}O_{10}$)$_2$(NO_3)$_2$](H_2O)$_2$}·12H_2O (**1**): TMeQ[6] (20.4 mg, 0.016 mmol), 4,4'-H_2BPs (10.48 mg, 0.033 mmol) and Ca(NO_3)$_2$ (1 mL, 23.6 mg/mL) were dissolved in 9 mL deionized water with stirring at room temperature. The solution was sealed in a Teflon-lined stainless-steel vessel and then heated at 180 ℃ for 10 h. After cooling down to room temperature, orange crystals of **1** were collected in 45% yield.

{[Sr($C_{30}H_{30}N_{20}O_{10}$)$_2$$Cl_2$]($NO_3$)$_2$($H_2O$)$_2$}·12$H_2O$ (**2**): TMeQ[6] (20.4 mg, 0.016 mmol), 4,4'-H_2BPs (10.48 mg, 0.033 mmol) and Sr(NO_3)$_2$ (1 mL, 21.1 mg/mL) were dissolved in 9 mL deionized water with stirring at room temperature. The solution was sealed in a Teflon-lined stainless-steel vessel and then heated at 180 ℃ for 10 h. After cooling down to room temperature, white crystals of **1** were collected in 42% yield.

{[Ba($C_{30}H_{30}N_{20}O_{10}$)$_2$(NO_3)$_2$](NO_3)$_2$(H_2O)$_2$}·12H_2O (**3**): TMeQ[6] (20.4 mg, 0.016 mmol), 4,4'-H_2BPs (10.48 mg, 0.033 mmol) and Ba(NO_3)$_2$ (1 mL, 26.1 mg/mL) were dissolved in 9 mL deionized water with stirring at room temperature. The solution was sealed in a Teflon-lined stainless steel vessel and then heated at 180 ℃ for 10 h. After cooling down to room temperature, white crystals of **1** were collected in 43% yield.

X-ray crystallography

Single crystal X-ray data were collected on a Bruker Apex-2000 diffractometer at 123 K using graphite monochromated Mo-K_α radiation (λ = 0.71073 Å) with ω/2θ scan mode. Lorentz-polarization and absorption corrections were applied. Structural solution and full matrix least-squares refinement based on F^2 were performed with the SHELXS-97 and SHELXL-97 program package[25-27], respectively. All the non-hydrogen atoms were refined anisotropically. The idealized positions of the hydrogen atoms were located by using 'riding' model with Uiso = 1.2 Ueq of carrier atom. Analytical expressions of neutral-atom scattering factors were employed, and anomalous dispersion corrections were incorporated. For these three complexes, owing to the high degree of disordered water molecules, the SQUEEZE routine of Platon was employed [28]. A summary of the crystallographic data, data collection and refinement parameters for complexes **1** - **3** is given in **table 1**.

Table 1. Crystal Data and Structure Refinements for **1**-**3** [a].

Compound	**1**	**2**	**3**
Chemical formula	$C_{64}H_{60}N_{24}O_{34}S_4Ca_2$	$C_{52}H_{51}N_{24}O_{22}S_2Sr$	$C_{64}H_{60}N_{24}O_{31}S_4Ba_2$
Formula weight	1917.76	1515.91	2064.28
Crystal system	Triclinic	Monoclinic	Triclinic
Space group	*P*-1	*P*21/c	*P*-1
a /Å	10.493(5)	20.282(5)	15.569(5)
b /Å	15.940(5)	15.713(5)	17.153(5)
c /Å	28.368(5)	24.849(5)	19.580(5)
α /°	95.591(5)	90.000(5)	106.089(5)
β /°	94.067(5)	101.101(5)	104.520(5)
γ /°	102.427(5)	90.000(5)	103.928(5)
Temperature /K	293(2)	293(2)	293(2)
Volume /Å^3	4591(3)	7771(3)	4585(2)
Z	2	4	2
D_c /g cm^{-3}	1.387	1.296	1.495
μ /mm^{-1}	0.307	0.828	1.033
F(000)	1976	3108	2072
Reflections	16089 / 9100	13681 / 7145	16088 /12276

Collected/unique Data / restraints / Parameters	16089 / 0 / 1157	13681 / 57 / 914	16088 / 0 / 1130
GOF	1.024	1.015	1.024
R_1, wR_2 $[I > 2\sigma(I)]$[a,b]	$R_1 = 0.0681$, $wR_2 = 0.1798$	$R_1 = 0.1100$, $wR_2 = 0.2208$	$R_1 = 0.0377$, $wR_2 = 0.0974$
R_1, wR_2 (all data)	$R_1 = 0.1151$, $wR_2 = 0.2001$	$R_1 = 0.1645$, $wR_2 = 0.2387$	$R_1 = 0.0521$, $wR_2 = 0.1033$

[a] $R_1 = \Sigma||F_o| - |F_c||/\Sigma|F_o|$. [b] $wR_2 = |\Sigma w(|F_o|^2 - |F_c|^2)|/\Sigma|w(F_o)^2|^{1/2}$, where $w = 1/[\sigma^2(F_o^2) + (aP)^2 + bP]$. $P = (F_o^2 + 2F_c^2)/3$

Luminescence Study

The crystal samples were ground well into a powder so as to improve the detecting efficiency. The samples were dissolved in deionized water (1 mg/mL) at room temperature because they keep stable in water. The solution was stirred at a constant rate in order to maintain homogeneity. All antibiotics were dissolved in acetonitrile and applied to add to analytics. In all fluorescence experiments, the excitation wavelength of supramolecular assemblies was 264 nm, and emission spectra were tested in the range of 284-508 nm.

Results and Discussion

Structural description

Description of structure of complex 1. Addition of 4,4'-biphenyldisulfonate (H_2BPDS) to TMeQ[6] in the presence of $Ca(NO_3)_2$ resulted in the formation of the complex $[Ca(C_{30}H_{30}N_{20}O_{10})_2(NO_3)_2](H_2O)_2$ (**1**). The single-crystal X-ray diffraction analysis revealed that complex **1** features a one-dimensional coordination polymer with a tubular structure. Complex **1** belongs to a low-symmetrical triclinic crystal system with a space group of *P*-1. There are two independent Ca^{2+} ions, one TMeQ[6] macrocycle ligand, two 4,4'-biphenyldisulfonate anions ($BPDS^{2-}$), ten coordinated water molecules, and fifteen lattice water molecules in the asymmetric unit. As depicted in **Fig. 1**, each Ca^{2+} ion is octacoordinated and adopts a trigon-dodecahedron coordination geometry. For example, the Ca(1) ion coordinates to three carbonyl groups (O1, O2, and O10) of adjacent TMeQ[6] ligands and five water molecules (O1w-O5w). The bond lengths for Ca(1)–O (carbonyl) and Ca(1)–O (water) are 2.4189(10)–

2.4658(11) and 2.4032(5)–2.6521(4) Å, respectively. The O–Ca(1)–O bond angles vary from 77.81° to 145.9°.

The most remarkable feature in complex **1** is that each TMeQ[6] macrocycle is bound to four Ca^{2+} ions and each Ca^{2+} ion is coordinated by two adjacent TMeQ[6] macrocycles, leading to the formation of a one-dimensional coordination polymeric chain (**Fig 1**). In this 1:2 ligand/metal polymeric chain, two Ca^{2+} cations between two TMeQ[6] ligands are separated by 10.805 Å. Note that the 1D coordination polymeric chain is surrounded by numerous $BPDS^{2-}$ anions. All these $BPDS^{2-}$ anions are not involved in metal ion coordination because the Ca^{2+} ion preferentially coordinates to TMeQ[6] ligands and water molecules. However, they connect with two neighboring polymeric chains through C–H···π (2.654 Å) interactions between the methylene groups of the TMeQ[6] macrocycles and the aromatic ring of the $BPDS^{2-}$, which has been termed "outer-surface interactions" by Tao *et al*[29]. In such a way, the TMeQ[6]-based polymeric chains extend to form a 2D layer on the *ab* plane (Fig. 1). Adjacent 2D layers are packed orderly along the *a*-axis to form a 3D supramolecular assembly (Fig. 1). Remarkably, the polycationic chains are arranged in a honeycomb structure with 1D channels extending along the *a*-axis. Thus, there are two kinds of 1D channels in the solid state, one being an intramolecular channel and the other one being an intermolecular channel.

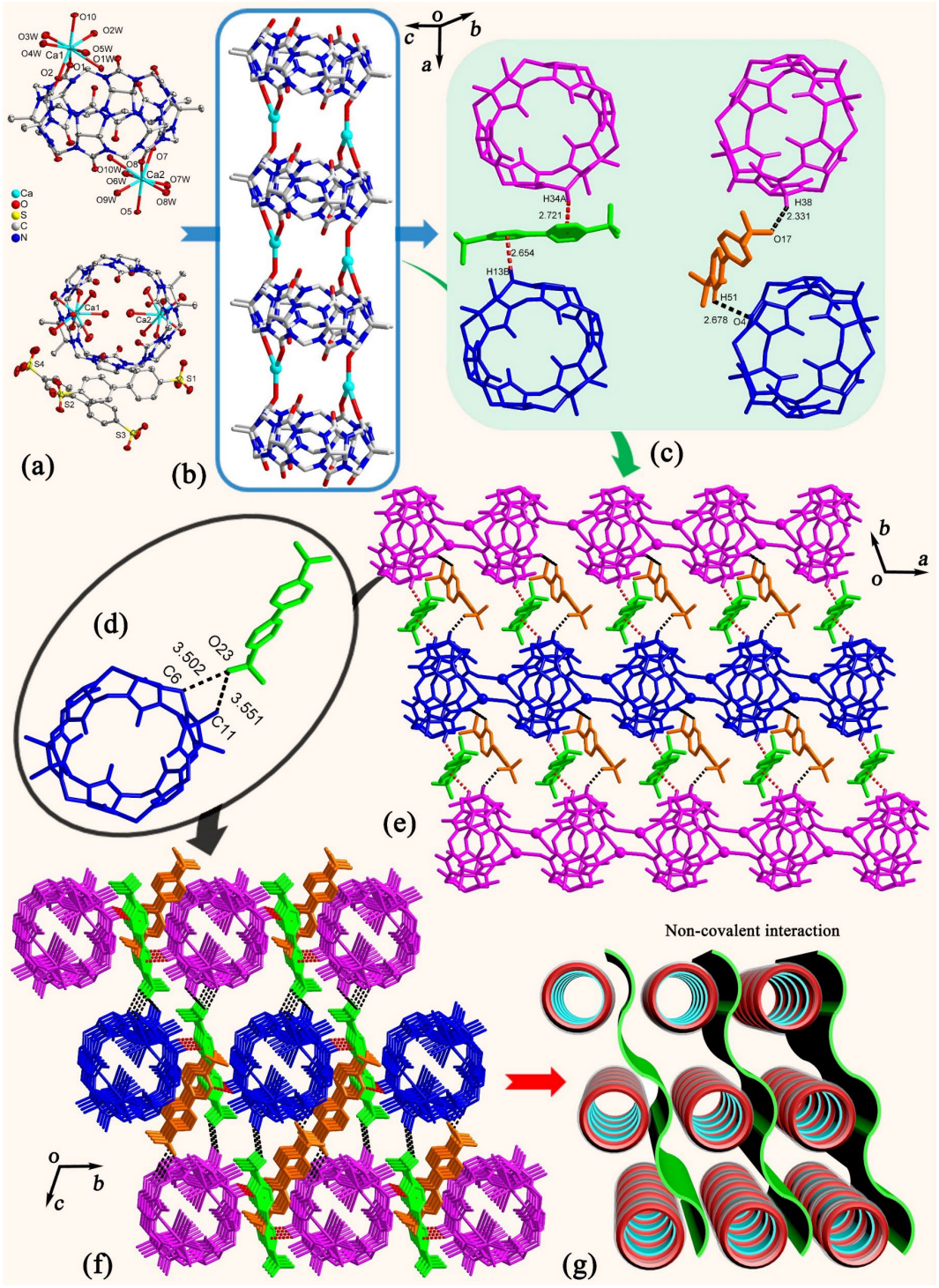

Figure 1. (a) The asymmetric unit of **1**; (b) The 1D TMeQ[6]-Ca^{2+}chain in **1**; (c) the C-H···π interaction between the ligand and TMeQ[6]; (d) Hydrogen bonding between the ligand and TMeQ[6]; (e) the 2D network of **1**; (f) the 3D architecture of **1**; (g) Schematic model of **1**. Note: H atoms and water molecules are omitted for clarity.

Description of structure of complex 2. Complexes **2** and **3** were prepared by the same method as complex **1**, but strontium and barium salt were used respectively. The X-ray crystallography confirmed that complex **2** features a one-dimensional coordination polymer with a zigzag-like structure. The structure crystallizes in the monoclinic system, space group P21/c. The asymmetric unit of complex **2** contains one half of TMeQ[6] ligand, one Sr(II) ion, one $BPDS^{2-}$ anion, four coordinated water molecules, and 10 lattice water molecules. As shown in Figure 3, the octacoordinated Sr(II) center adopts trigon-dodecahedron coordination geometry. The Sr(1) ion is coordinated by four carbonyl oxygens (O1, O2, O7, and O12#1) from different TMeQ[6] ligands, and four water molecules (O1w, O2w, O3w, and O4w). The Sr-O bond lengths vary from 2.510(5) to 2.7188(5) Å and the O–Ca(1)–O bond angles are in the range of 75.4°-144.7°.

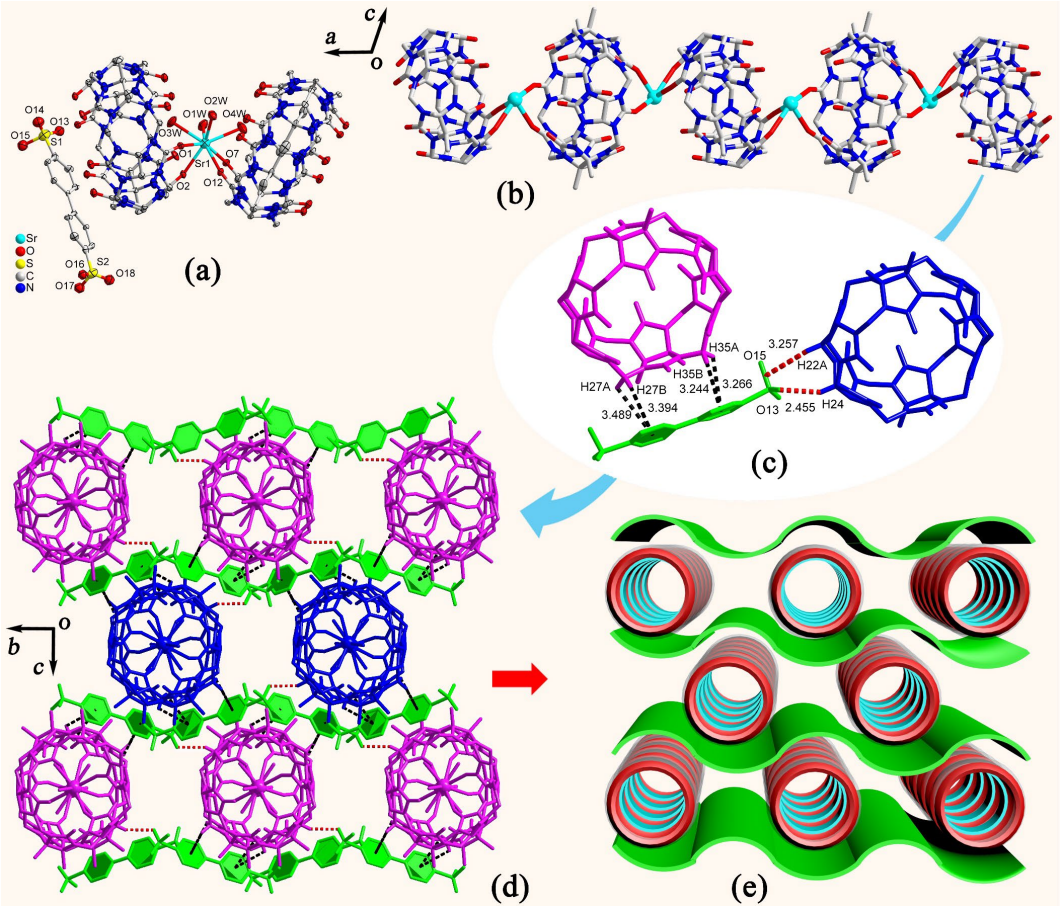

Figure 2. (a) The asymmetric unit of **2**; (b) The 1D TMeQ[6]-Sr^{2+}chain in **2**; (c) the interaction between the ligand and TMeQ[6]; (d) the 3D architecture of **2**; (g) Schematic model of **2**. Note: H atoms and water molecules are omitted for clarity.

Concomitantly, each of the TMeQ[6] ligands adopts a bis-bidentate coordination mode and connects two Sr(II) ions. It is noteworthy that adjacent TMeQ[6] ligands are not parallel to each other. Measured along the equator of the TMeQ[6], the dihedral angle of two neighboring

TMeQ[6] ligands is 37.34° (Figure 5a). Thus, the coordination of TMeQ[6] with Sr(II) ion produces an infinite *zigzag* polymeric chain (Figure 2a), of which surround numerous deprotonated $BPDS^{2-}$. In complex **2**, as in complex **1**, the $BPDS^{2-}$ anion is not involved in metal ion coordination, but C–H···π (3.422 Å) interactions are present. These zigzag chains are parallel and are further bridged through the $BPDS^{2-}$ anions forming a 3D framework with 1D channels along the *b*-axis (Figure 5b). The guest water molecules occupy the void interspace region and interact with the coordinated water molecules of frameworks. PLATON calculated suggested a solvent-accessible volume of 96.2 $Å^3$ (approximately 8.2% of unit cell) by excluding the guest water molecules[30].

Description of structure of complex 3. The single-crystal structural analysis revealed that complex **3** consists of one-dimensional coordination polymer with a blocked tubular structure. Complex **3** belongs to the triclinical space group of *P*-1 with an asymmetric unit containing two crystallographically independent Ba^{2+} ions, one TMeQ[6] macrocycle ligand, two $BPDS^{2-}$ anions, seven coordinated water molecules, and 10 lattice water molecules. As can be seen in Figure 6, although Ba1 and Ba2 are both non-coordinated, they possess completely different coordination environments. The Ba1 ion coordinates to four carbonyl oxygens (O10, O11, O5#1 and O6#1, symmetry operation A = x - 1, y, z + 1) of adjacent TMeQ[6] ligands, three water molecules (O1w, O2w, and O7w) and one monodentate sulfonate oxygen atoms (O13) of the $BPDS^{2-}$ anion. Ba2 ion coordinates to three carbonyl oxygens (O1, O2, and O8) of adjacent TMeQ[6] ligands, and six water molecules (O1w-O6w). It should be noted that the two Ba ions are separated by 4.573(5) Å and are connected to each other through the coordination of three bridging water molecules (O1w, O2w, and O3w). The bond lengths of Ba–O vary in the range of 2.750(1)−3.023(4) Å, which are shown in Table S1.

The most distinguishing feature of complex **3** is that alternating $Ba_2(\mu_2\text{-}H_2O)_3(H_2O)_3BPDS^{2-}$ units and TMeQ[6] ligands along the same direction results in a one-dimensional coordination polymer (Figure 7). The coordination polymer chains are surrounded by six neighboring chains. In the solid-state of complex **3**, 1D channels are parallel to the *b*-axis and are filled with water molecules. Computation of these channels using PLATON suggests a value of 4488.0 $Å^3$, corresponding to 57.5% of the unit cell volume.[27]

Compared with complexes **1** and **2**, there are two different kinds of $BPDS^{2-}$ anions in complex **3**: one being free and the other one being coordinated with the metal ion. Both types have been incorporated into the formation of the "outer-surface interactions" with the neighboring TMeQ[6] macrocycles, which contribute to stabilizing the coordination polymers.

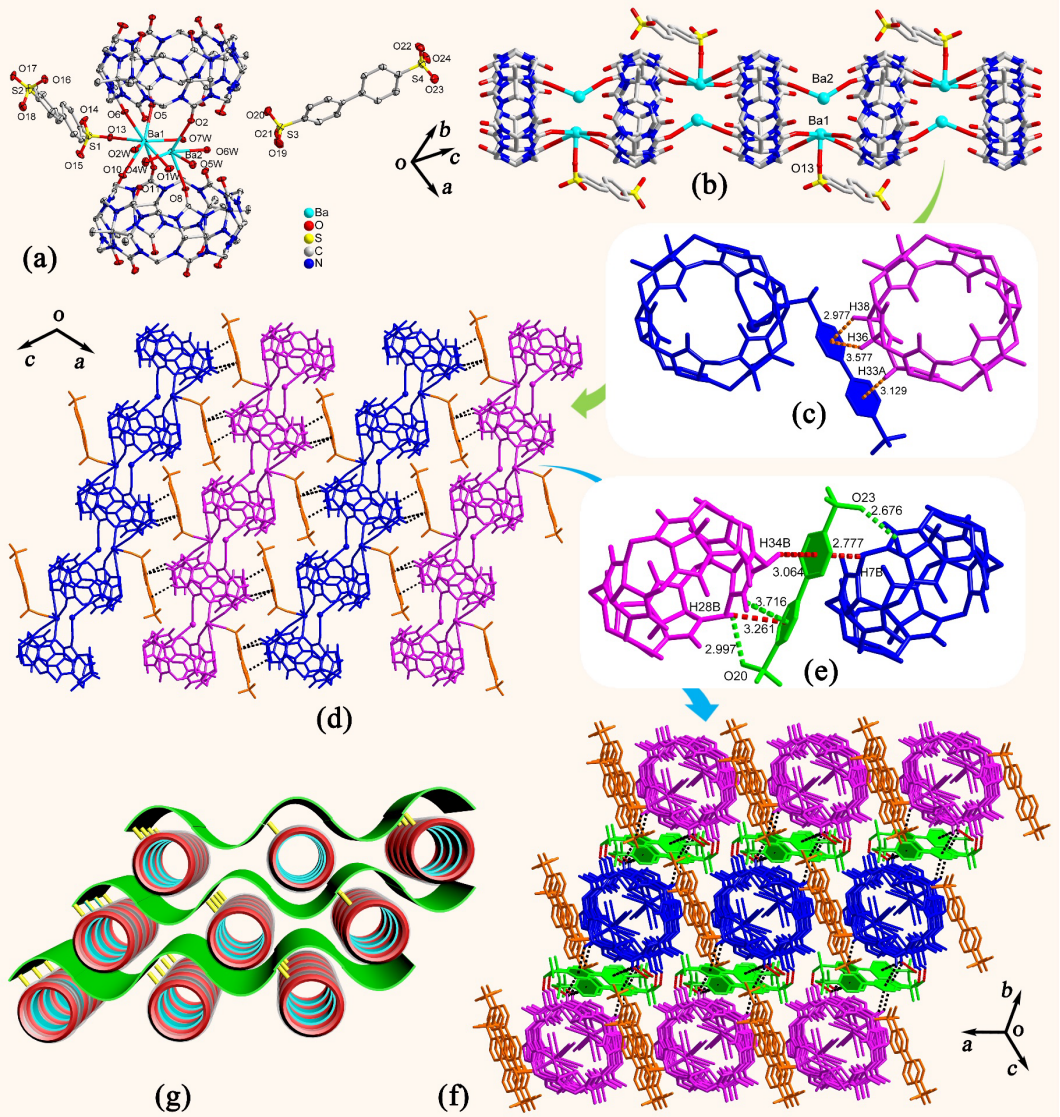

Figure 3. (a) The asymmetric unit of **3**; (b) The 1D TMeQ[6]-Ba^{2+}chain in **3**; (c) the C-H···π interaction between the ligand and TMeQ[6]; (d) the 2D network of **3**; (e) Hydrogen bonding between the ligand and TMeQ[6]; (f) the 3D architecture of **3**; (g) Schematic model of **3**. Note: H atoms and water molecules are omitted for clarity.

3.2. Roles of the $BPDS^{2-}$ in the complexes 1−3

As shown above, complexes **1**−**3** feature one-dimensional coordination polymers, but quite different architectures. There is no doubt that the $BPDS^{2-}$ anion plays a remarkable role in the construction of these coordination polymers. As a matter of fact, without the assistance of any third species, the coordination of TMeQ[6] with Ca(II) produces discrete complex {TMeQ[6]·[CaCl]}·[Cl]·17.5H_2O.[31] On the one hand, the $BPDS^{2-}$ acts as a counter anion that balances the charge of these complexes. Moreover, the $BPDS^{2-}$ anion is an auxiliary ligand with a certain structural function. In complexes **1** and **2**, the $BPDS^{2-}$ anion is not involved in the

coordination with the metal ion, but is incorporated into the "outer-surface interactions" to stabilize the coordination polymers. In the case of complex **3**, one of the two $BPDS^{2-}$ anions displays a monodentate and terminal coordination mode. Although the $BPDS^{2-}$ anion possesses two sulfonic acid groups, it fails to link adjacent 1D polymers by a coordination interaction to form 2D plane structure. This is probably because the $BPDS^{2-}$ anion is not long enough.

3.3. Photoluminescence properties

The solid-state fluorescence spectra of TMeQ[6] and 4,4'-biphenyldisulfonate (H_2BPDS) were obtained at λ_{ex}=230 nm. As shown in **Fig. 4**, the ligand shows a strong emission peak at 344 nm and TMeQ[6] shows emission at 362, 424, 460, and 497 nm. The fluorescence spectra of **1**, **2**, and **3** in aqueous suspension were obtained at λ_{ex}= 264 nm. The emission peaks of **2** and **3** were observed at 318 nm, while the emission peaks of **1** were observed at 319 nm and 423 nm. It is interesting to observe **1** appearing at a small peak at 423 nm. The wavelength of complex **1** may be attributed to TMeQ[6].

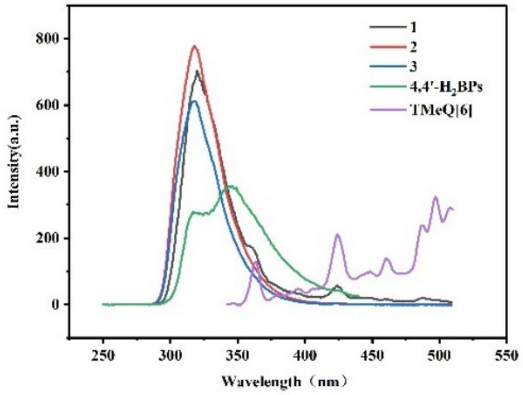

Figure 4. Fluorescence spectra of **1**, **2**, and **3** in an aqueous suspension, H_2BPs, and TMeQ[6] in the solid state at room temperature.

3.4. Detection of antibiotics

Complexes **1**, **2** and **3** have excellent fluorescence, which allows us to explore the possibility of using them as fluorescence sensor materials. Before the sensing experiments, the assemblies were ground into powders and then soaked in deionized water to form a stable suspension (1 mg/ml). Finally, the fluorescence intensity of the suspension (3 ml) was investigated by adding different antibiotics (100 μL) to the solution. The types of antibiotics include Norfloxacin (NFX), Nitrofurantoin (NFT), Nitrofurazone (NFZ), Metronidazole (MDZ), Chloramphenicol (CAP), Amoxicillin (AMX), Sulfapyridine (SASP), Sulfadiazine (SD), Sulfamethoxazole (SMZ). Antibiotics have different influences on the supramolecular assembly suspension. The quenching efficiency was calculated by the equation $(I_0\text{-}I)/I_0*100\%$ (I_0 means the fluorescence of the initial

sample, I mean the fluorescence after the addition of antibiotics). The results indicate that the fluorescence emissions of assemblies were quenched mostly in the presence of NFX, while fluorescence intensity was just slightly influenced by the addition of other antibiotics.

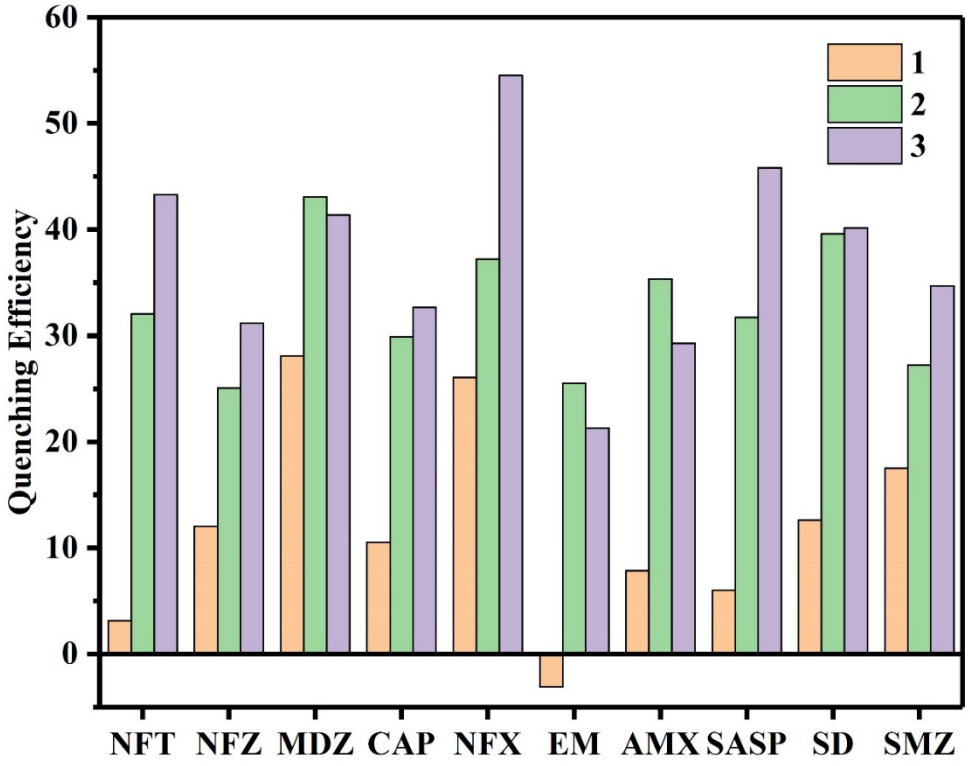

Figure 5. The variation of the quenching efficiency of the suspensions of **1**, **2**, and **3** upon the addition of different antibiotics (Orange: **1**, Green: **2**, Purple: **3**)

Moreover, to further explore the sensitivity of the assemblies towards NFX, concentration-related experiments were conducted. As shown in **Fig. 6**, it was found that the fluorescence intensities of complexes **1**, **2**, and **3** decreased gradually with the incremental addition of NFX. The NFX could entirely quench the fluorescence of the complex. What is interesting is that the wavelength of complex **1** decreased at 319 nm and 423 nm, but intensified at 450 nm. By contrast, this did not happen for the complexes **2** and **3**. From the picture inserted in **Fig. 6**, it can be clearly seen that the color of compound **1** changed under 256 nm. The wavelength of **2** and **3** just decreased at 318 nm. This clearly indicates that **1** has good sensitivity towards NFX.

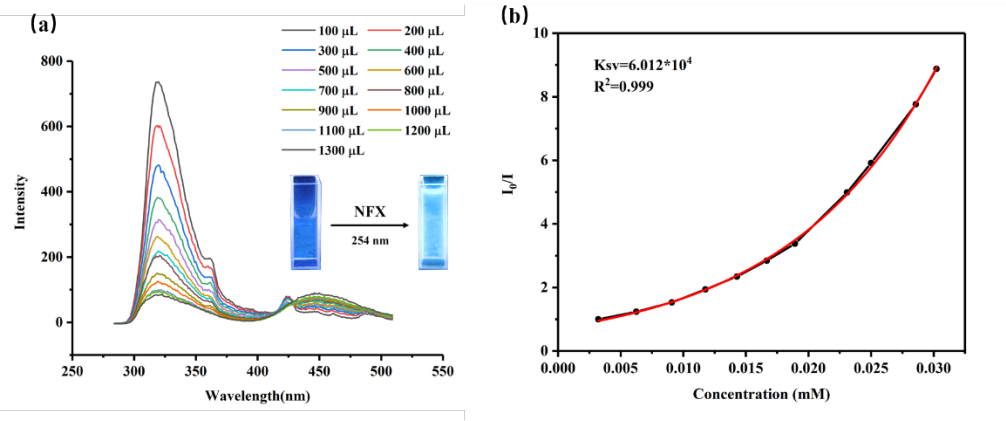

Figure 6. Change in emission intensities of **1** with the gradual addition of NFX (a) and the fit curve (b), picture insert: the suspension of **1** before and after adding NFX under 254 nm.

The fluorescence quenching efficiencies and constants for the NFX were analyzed by plotting the relative intensities (I_0/I) against the concentration of NFX. The results show that the plots were bent upwards. This indicated that the quenching occurred via a different mechanism, including a static pathway or a combination of static and dynamic pathways[32]. It is well known that the mechanism of fluorescence quenching can be determined by measuring the fluorescence lifetime of the complex. Through understanding of the fluorescence lifetime of the complex (**Fig. S7**), we found that the fluorescence life of compounds **2** and **3** did not change significantly [33,34]. This shows that complexes **2** and **3** follow the Stern-Volmer equation: $I_0/I=Ae^{K[Q]}+B$ (A, B, and K are constants, the quenching constants $K_{sv}=A*K$). According to the equation, $DL=3\sigma/m$ (σ is the standard deviation and m is the slope). The detection limit (DL) was estimated to be $9.52*10^{-4}$ and $2.55*10^{-4}$. Additionally, recycling experiments were carried out, and it was found that samples can be recovered at least five times after acetonitrile washing and centrifugation (**Fig. S8**).

While complex **1** had a longer fluorescence lifetime (**Fig. S7**), it did not remain constant. The interesting phenomenon inspired us to explore the mechanism of the fluorescence quenching. Firstly, complex **1** was immersed in 0.02 M NFX solution, and its PXRD was recorded after drying. The PXRD results were compared with the original experimental results, and slight changes were found in compound **1**, but the overall skeleton did not change, as can be seen from the comparison of experimental results (**Fig. S9**). In addition, no new functional group structure was found through the comparison of infrared spectra (**Fig. S10**). The photoinduced electron transfer (PET) mechanism is probably the main reason. The 4,4'-H_2BPs ligand has a strong π-conjugated effect and the analytes are electron deficient [35,36]. The quenching phenomenon may result from the transportation of excited electrons. The fluorescence ligand has the higher lowest

unoccupied molecular orbit (LUMO) and the analytes have the lower unoccupied molecular orbit (LUMO). The frontier orbital of the antibiotics have been reported in the literature, and the NFX show lower energy levels. [35,37-38] Besides that, the effective FRET process from complex to the antibiotics may also result in fluorescence quenching. The absorption spectra of NFX has an overlap with the excitation of the complex **1 (Fig. S11)**[39]. However, the PET and FRET theory only explains the phenomenon of fluorescence quenching at 319nm, but does not explain the phenomenon of enhancement at 450 nm. The possible explanation for this is that the quencher and the fluorescent substance undergo a coordination reaction in the ground state, and the resulting complex is usually non-luminescent, but in this phenomenon, the complex is luminescent. This also explains why the fluorescence lifetime becomes longer. In addition, the blue shift of the absorption spectrum of **1** can also prove the formation of new complexes[40] (**Fig. S12**). Therefore, the above results indicate that PET and FRET play an important role of fluorescence quenching and that the formation of the new complex involves fluorescence enhancement.

Conclusion

In summary, we have characterized three one-dimensional coordination polymers of alkali-earth metal ions (Ca^{2+}, Sr^{2+}, and Ba^{2+}) with the TMeQ[6] and the $BPDS^{2-}$ anions. In these three complexes, the deprotonated BPDS not only acts as a counter anion that balances the charge of these complexes, but also forms "outer-surface interactions" with the TMeQ[6] to stabilize the coordination polymers. In addition, the bipyridine ligand is not involved in the coordination with the Ca^{2+} and Sr^{2+}, but is with the Ba^{2+} metal ions. The present study sheds light on the design and construction of Q[*n*]-based poly-dimensional coordination polymers through addition of a third species. Sensing experiments indicate that complex **1** is a promising fluorescence probe for detecting antibiotics (NFX) with a low limit of detection. This work might prove that Q[*n*]-SOFs would have the potential application in the detection of environmental pollutions.

Supplementary materials

CCDC 2036196-2036198 contain the supplementary crystallographic data for this paper. The data can be obtained free of charge via www.ccdc.cam.ac.uk/data_request/cif (or from The Cambridge Crystallographic Data Centre, 12, Union Road, Cambridge CB2 1EZ, UK; fax: +44 1223 336 033; e-mail: deposit@ccdc.cam.ac.uk).

Acknowledgments

We acknowledge the support of National Natural Science Foundation of China (No. 21601090, 21761007 and 21871064), and the Natural Science Foundation of Jiangsu Province (Grant No. BK20160943). Dr. K. Chen thanks Major Project of Basic Science (Natural Science) Research in Higher Education Institutions of Jiangsu Province (22KJA150002). CR thanks the University of Hull for support.

References

1. H. Douafer, `V. Andrieu, O. t. Phanstiel, J. M. Brunel, J Med Chem, 2019, **62**, 8665-8681.
2. X. Q. Yang, P. P. Xia, Y. Zhang, S. Q. Lian, H. F. Li, G. Q. Zhu, P. F. Wang, ACS Appl. Bio Mater, 2020, **3**, 5395-5406.
3. S. Hess, D. Kneis, T. Osterlund, B. Li, E. Kristiansson, T. U. Berendonk, Environ. Sci. Technol. 2019, **53**, 13898-13905.
4. U. Sharaha, E. R. Diaz, K, Riesenberg, I. J. Bigio, M. Huleihel, A. Salman, Anal. Chem, 2017, **89**, 8782-8790.
5. Z. Q. Ye, H. S. Weinberg, Anal. Chem, 2007, 79, 1135-1144.
6. J. H. Sun, A. R. Warden, J. Huang, W. Y. Wang, X. T. Ding, Anal. Chem. 2019, **91**, 7524-7530.
7. X. G. Yang, X. M. Lu, Z. M. Zhai, J. H. Qin, X. H. Chang, M. L. Han, F. F. Li, L. F. Ma, Inorg. Chem. Front, 2020, **7,** 2224-2230.
8. X. M. Tian, S.L. Yao, C. Q. Qiu, T. F. Zheng. Y. Q. Chen, H. P. Huang, J. L. Chen, S. J. Liu, H. R. Wen, Inorg. Chem. Front, 2020, **59**, 2803-2810.
9. Y. J. Ma, J. X. Hu, S. D. Han, Han, J. Pan, J. H. Li, G. M. Wang, J. Am. Chem.Soc. 2020. **142**, 2682-2689.
10. W.K. Yang, Y.H. Yang, H.H. Li, D.Y. Lin, W.T. Yang, D.Y. Guo, Q.H. Pan, Inorg. Chem. Front, 2020, **7**, 3718–3726.
11. X.D. Qin, W.T. Yang, Y.H. Yang, D.X. Gu, D.Y. Guo, Q.H. Pan, Inorg. Chem, 2020, **59**, 9857–9865.
12. H.H. Li, W.T. Yang, Q.H. Pan, RSC Adv, 2020, **10**, 33879–33893.
13. S.L. Yao, S.J. Liu, X.M. Tian, T.F. Zheng, C. Cao, C.Y. Niu, Y.Q. Chen, J.L. Chen, H.P. Huang, H.R. Wen, Inorg. Chem, 2019, **58**, 3578–3581.

14. Y.Q. Chen, Y. Tian, S.L. Yao, J. Zhang, R.Y. Feng, Y.J. Bian, S.J. Liu, Chem.-Asian J, 2019, **14** 4420–4428.
15. B. Wang, P.L. Wang, L.H. Xie, R.B. Lin, J. Lv, J.R. Li, B.L. Chen, Nat. Commun, 2019, **10,** 3861.
16. X.D. Zhang, G.J. Ren, M.L. Li, W.T. Yang, Q.H. Pan, Cryst. Growth Des, 2019, **19**, 6308–6314.
17. X. L. Ni, X. Xiao, H. Cong, L. L. Liang, K. Cheng, X. J. Cheng, N. N. Ji, Q. J. Zhu, S. F. Xue, Z. Tao, Chem. Soc. Rev., 2013, **42,** 9480.
18. J. Lagona, P. Mukhopadhyay, S. Chakrabarti and L. Isaacs, Angew. Chem., Int. Ed., 2005, **44**, 4844.
19. E. Masson, X. Ling, R. Joseph, L. Kyeremeh-Mensah and X. Lu, RSC Adv., 2012, **2**, 1213.
20. A. E. Kaifer, Acc. Chem. Res., 2014, **47**, 2160.
21. S. J. Barrow, S. Kasera, M. J. Rowland, J. Barrio and O. A. Scherman, Chem. Rev., 2015, **115**, 12320.
22. K. I. Assaf and W. M. Nau, Chem. Soc., Rev. 2015, **44**, 394.
23. J. Murray, K. Kim, T. Ogoshi, W. Yao and B. C. Gibb, Chem. Soc. Rev., 2017, **46**, 2479.
24. Y. J. Zhao, S. F. Xue, Q. J. Zhu, Z. Tao, J. X. Zhang, Z. B. Wei, L. S. Long, M. L. Hu, H. P. Xiao, A. I. Day, Chin. Sci. Bull. 2004, **49**, 1111–1116.
25. G. M. Sheldrick, SHELXS-97, Program for X-ray Crystal Structure Determination, University of Göttingen, Germany, 1997;
26. G. M. Sheldrick, SHELXL-97, Program for X-ray Crystal Structure Refinement, University of Göttingen, Germany, 1997;
27. G. M. Sheldrick, Acta Crystallogr., Sect. A, 2008, **64**, 112-122.
28. A. L. Spek, J. Appl. Crystallogr., 2003, 36, 7-13.
29. Ni, X.L., Xiao, X., Cong, H., Zhu, Q.J., Xue, S.F., Tao, Z.: *Acc. Chem. Res.*, 2014, **47**, 1386–1395.
30. A. L. Spek, PLATON, A Multi purpose Crystallographic Tool; Utrecht University: Utrecht, The Netherlands, 1998.
31. Y.Q. Zhang, L.M. Zhen, D.-H. Yu, Y.-J. Zhao, S.-F. Xue, Q.-J. Zhu, Z. Tao, J. Mol. Struct. 2008, **875**, 435–441.
32. L.H. Cao, F. Shi, W.M. Zhang, S.Q. Zang, C. W. Mak. Thomas, Chem. Eur. J. 2015, **21**, 15705–15712.
33. X.H. Zhou, H.H. Li, H.P. Xiao, L. Li, Q. Zhao, T. Yang, J.L. Zuo, W. Huang, Dalton Trans, 2013, **42**, 5718–5723.

34. F. Zhang, Y. Wang, T. Chu, Z. Wang, W. Li, Y.Y. Yang, Analyst, 2016, **141**, 4502–4510.
35. X.D. Zhu, K. Zhang, Y. Wang, W.W. Long, R.J. Sa, T.F. Liu, J. Lü, Inorg. Chem, 2018, **57**, 1060–1065.
36. M.K. Yu, Y. Xie, X.Y. Wang, Y.X. Li, G.M. Li, ACS Appl. Mater. Inter, 2019, **11**, 21201–21210.
37. S.L. Sun, X.Y. Sun, Q. Sun, E.Q. Gao, J.L. Zhang, W.J. Li, J Solid State Chem, 2020, **292**, 121701.
38. Z. W. Zhai, S. H. Yang, M. Cao, L.K. Li, C.X. Du, S.Q. Zang, Cryst. Growth Des, 2018, **18**, 7173–7182.
39. S. S. Nagarkar, B. Joarder, A.K. Chaudhari, S. Mukherjee, S.K. Ghosh, Angew. Chem. Int. Edit, 2013, **52**, 2881–2885.
40. M. Yagishita, S. Ohshima, Polycycl. Aromat. Compd, 2012, 32(2), 188-198.

Synopsis

4,4’-Biphenyldisulfonic acid induced coordination polymers of symmetrical tetramethyl cucurbit[6]uril with alkaline-earth metals for detection of antibiotics

Kai Chen[a]*, Zhao-Qiang Zhu[a], Ming-Hui Zhang[a], Chen Chen[a], Jing-Xin Liu[b]*, Jing-Xin Liu[b]* Carl Redshaw[d]

Three one dimensional coordination polymers of alkali-earth metal ions (Ca^{2+}, Sr^{2+} and Ba^{2+}) with the TMeQ[6] and the 4,4’-biphenyldisulfonate anion were characterized, which provides a strategy to construct poly-dimentional coordination polymers.